Generation IV_GFR Materials Program

FY-2006 Summary Report:

Proton Irradiation Study of GFR Candidate Ceramics

Jian. Gan[1]and Todd Allen[2]

[1]Idaho National Laboratory
[2]University of Wisconsin

October 24, 2006

Abstract

This is a 1-year program to investigate the microstructural changes in GFR candidate ceramics due to proton irradiation. It continues the previous work on the same set of ceramics which used heavy ion irradiation. There are 5 ceramics (ZrC, ZrN, TiC, TiN and 6H-SiC) irradiated with 2.6 MeV protons at a temperature of 800ºC to a single dose for each ceramic in the range of 1.5 to 3.0 dpa depending on the material. Post-irradiation examination reveals the microstructural changes due to proton irradiation. The change of lattice constant evaluated using HOLZ patterns is not observed for the irradiated samples up to 1.5 dpa for 6H-SiC and up to 3.0 dpa for ZrC and ZrN. In contrast to Kr ion irradiation at 800ºC to 10 dpa, the proton-irradiated ceramics at 3.0 dpa show less irradiation damage to the lattice structure evidenced by the visibility of the HOLZ line pattern and Kikuchi pattern. The irradiated ZrC exhibits faulted loops which are not observed in the Kr ion irradiated sample. The irradiated ZrN shows the least microstructural change from proton irradiation. The microstructure of 6H-SiC irradiated to 3.0 dpa consists of black dot type of defects at high density.

Introduction

Refractory ceramics have been considered for the gas cooled fast reactor (GFR) because of their high temperature stability at approximately 1000°C under normal operation and up to 1600ºC during a loss of coolant accident. Refractory ceramics of ZrC, ZrN, TiC, TiN and SiC are candidates for both structural and fuel matrix materials due to their neutronic performance, thermal properties, chemical behavior, crystal structure, and physical properties. The transition metal carbides and nitrides (ZrC, ZrN, TiC and TiN) have a NaCl type FCC structure. The 6H-SiC is a common form of SiC that has a hexagonal structure. The crystal structures of these ceramics are shown in Figure 1. The high dose radiation effects on the microstructure of these ceramics have been previously explored using Kr ion irradiation at 800ºC. Proton irradiation of these ceramics has not been investigated before. It is believed that by using both heavy ion and proton irradiation at relevant conditions, the microstructural response under neutron irradiation in a GFR environment can be anticipated.

A literature review of radiation effects in ceramics can be found in the previous report on heavy ion irradiation study of GFR ceramics [1]. In summary, a volume increase of roughly 2% and 2.5% were observed in TiC and ZrC, respectively, when irradiated in the Engineering Test Reactor (ETR) at 130-355ºC to 7.5 dpa [2]. Post-irradiation thermal annealing indicated a greater shrinkage effect in TiC than in ZrC, suggesting a larger fraction of single defects in TiC. The smaller volume increase in TiC from irradiation was attributed to a smaller fraction of defect clusters compared to ZrC. The single defects are believed to cause less volume increase than clusters and are relatively easier to be annealed out.

SiC is a special material due to its electronic properties, thermal stability, extreme hardness and chemical inertness. The work by Weber, et al., [3] on single crystal 6H-SiC irradiated in-situ along the [0001] orientation with 1.5 MeV Xe ions at low temperatures (20K~475K) revealed that the material becomes completely amorphous at a dose of 0.25 dpa at T=20K. They found the critical temperature above which amorphization does not occur is 485K. Persson et al., reported their work on 4H-SiC implanted with 180 KeV Al ions at 600°C to doses of $1.3\sim7.8\times10^{14}$ cm^{-2}. They found loops at doses above 2.6×10^{14} ions/cm^2 and the loops reside on the (0001) basal plane with average size of approximately 50 nm [4]. They also reported that the loops in 4H-SiC consist of C or Si self-interstitials, or both [5].

The previous work on Kr ion irradiation of the GFR candidate ceramics reveals that 6H-SiC has the most stable microstructure among the 5 materials although dislocation loops are present at 70 dpa. TiC and TiN perform better than ZrC and ZrN. Perfect loops are found in both TiC and TiN, but not in ZrC and ZrN. Void swelling is not found in any of the 5 ceramics even at 70 dpa. At an irradiation temperature of 800ºC, no radiation-induced amorphization was found up to 70 dpa. While ring patterns are observed in ZrC, an ordered fcc (LI_2) microstructure is identified in ZrN at 70 dpa. The lattice expansion due to irradiation in TiC or TiN is approximately a factor of 4 lower than in ZrC or ZrN. The absolute value from the lattice constant evaluation is not so reliable due to the use of selected area diffraction since the more accurate measurement using higher order Laue zone (HOLZ) patterns is not available for those sample conditions.

This work investigated the microstructural response of ZrC, ZrN, TiC, TiN and SiC irradiated with 2.6 MeV protons at 800ºC. Proton irradiation at this energy will produce a uniformly damaged layer with depth more than 30 μm. This provides great advantage over the Kr ion irradiation where the effective sample depth is approximately less than 300 nm. The formation of surface oxides in Kr irradiation could create a severe problem on the irradiated sample for microstructure analysis using TEM. The proton irradiated ceramics can be made into TEM samples by using a middle section of the damaged layer with fresh and clean surface on both sides, completely eliminating the surface oxidation problem. This is important to reduce the complexity and confusion in microstructure characterization particularly for irradiated samples.

Experiments

All the 5 candidate ceramics, ZrC, ZrN, TiC, TiN and α-SiC, are commercial grade made by CERCOM in the US. These ceramics are produced by vacuum hot pressing of powders and

then machining to form rods. Their chemical compositions are listed in Table 1. The densities measured from the previous study are listed in Table 2. The 3 mm diameter discs with a thickness of 300 μm were cut using a low speed diamond saw. These disc samples were then wet-polished down to a fine surface finish before irradiation.

Table 1. Chemical composition of the refractory ceramics (wt%)

	Zr	Ti	Si	Hf	Zn	W	C	N	O	Others	Ratio*
ZrC	**84.8**	0.19	<0.001	1.91	<0.02	<0.1	**11.3**	0.61	0.21	<0.1	1.01
ZrN	**87.6**	0.095	0.007	<0.02	<0.02	0.19	0.76	**11.4**	1.43	<0.1	0.85
TiC	<0.02	**80.2**	0.007	<0.02	0.17	<0.05	**19.4**	0.057	0.51	<0.02	0.97
TiN	<0.02	**78.9**	0.001	<0.02	<0.02	<0.05	0.58	**22.0**	0.46	<0.02	0.95
SiC	<0.005	<0.1	**62.08**	<0.005	<0.001	<0.05	**29.6**	0.35	0.58	Al_1.44 Fe_0.65	1.11

* The atomic ratio of the major element C or N to Zr, Ti or Si.

Table 2. Results of density measurement for as-received ceramics (g/cm^3)

Ceramics	By dimension	By immersion	Theoretic	Imm./Theoretic (%)
ZrC	6.59	6.58	6.48	101.5
ZrN	7.06	7.06	7.30	96.7
TiC	4.84	4.84	4.90	98.8
TiN	4.43	4.92	5.39	91.3
SiC	3.18	3.19	3.22	99.1

The irradiation was conducted with 2.6 MeV protons using a Tandem accelerator at the University of Wisconsin. All of the 5 ceramics are irradiated in the same irradiation batch with 3 discs for each ceramics mounted on the irradiation stage, as shown in Figure 2 along with the damage depth profiles calculated from TRIM [[6]]. TEM disc samples were irradiated at 800 ± 15ºC to doses of 1.5 dpa for SiC, 2.5 dpa for TiC (or TiN) and 3.0 for ZrC (or ZrN). After irradiation, all the irradiated discs were transferred to Idaho National Laboratory. Samples are visually inspected using an optical microscope. It was found that all the TiN discs have a surface cracking problem and most of the irradiated surface area is missing, as shown in Figure 3. This possibly occurred near the end of the irradiation judging by the color difference between the fresh surface and the residual irradiated area. Therefore, the analysis for the irradiated TiN is not available for this report. Follow-on work at the University of Wisconsin using profilometry indicate the depth at which the surface fracture occurred is very close to the calculated irradiation depth.

The TEM sample preparation for microstructural anaysis is illustrated in Figure 4. The discs were mechanically polished from the unirradiated side down to a thickness of approximately 100 μm followed by dimple grinding from the same side to stop at roughly 30 μm from the irradiated side. The discs were then ion polished from both sides till perforation with 5 keV Ar ions at an incident angle of 7 degree using a Gatan Model 691 precision ion polishing system. Since the depth of the uniformly damaged layer for 2.6 MeV protons is 30-40 μm, shown in Figure 2, this ensures the perforation occurred at the flat region in the damage profile around 15 μm from the irradiated side. The thin area around the perforation was used for the TEM analysis.

Post-irradiation microstructural characterization was conducted at INL using a JEOL2010 transmission electron microscope operated at 200 kV. The features of the irradiated microstructure such as loops, dislocation network, cavities and precipitates were examined. Diffraction patterns at major zone axes such as [011] or [001] were recorded for ceramics with a fcc crystal structure (ZrC, ZrN, TiC and TiN). Two beam diffraction at **g**=(200) is used for bright field imaging of dislocations and loops while rel-rod dark field imaging is used to examine if faulted loops were present. For the hexagonal 6H-SiC, the diffraction patterns at zone [1,-2,1,0], [0,2,-2,-1] and [0,0,0,1] are used to determine the possible lattice expansion while the diffraction of (0,0,6) or (2,-1,6) near zone [0,-1,1,0] or [1,-2,1,0] are used for the loops. The high resolution images for 6H-SiC basal plane projection are obtained at zone [1,-2,1,0] without the objective aperture.

It is realized that the use of higher order Laue zone (HOLZ) pattern in convergent beam electron diffraction allows the accurate measurement of the lattice constant with an uncertainty of 0.2%. This is much better than the measurement using selected area diffraction patterns [7,8]. A HOLZ pattern simulation software was used to determine the lattice constant [9]. A single crystal Si sample with a known lattice constant of 0.5431 nm was used as a reference to calibrate the electron beam energy in the microscope. The higher order Laue zone line patterns were recorded for both unirradiated and the proton-irradiated samples. Determination of the HOLZ patterns for the Kr-ion irradiated samples from the previous work has been attempted without any success even for the 10 dpa condition due to the poor visibility of the pattern for those irradiation conditions.

Results

The results of density measurements are listed in Table 2 along with the theoretical density of these ceramics for comparison [10,11]. The higher density for ZrC (101.5%T.D.) and lower density for TiN (91.3%T.D.) is due to Hf (~2 wt.%) in ZrC and the porosity in TiN. As reported in the previous work on the Kr ion irradiation study, general features of the unirradiated microstructure for all 4 refractory ceramics are the uniformly distributed small defect clusters introduced by ion milling damage during sample preparation. These small defects are even present in samples ion polished at 3 keV and a 4 degree incident angle. For the ceramics irradiated with protons to 3.0 dpa, no voids were found in ZrC, ZrN and 6H-SiC. The following sections describe the microstructure analysis for these ceramics before and after irradiation with protons at 800ºC.

ZrC

The microstructure of the unirradiated and irradiated ZrC is shown in Figure 5. The unirradiated microstructure is dominated by a large number of small black dots due to ion milling with 5 KeV Ar ions. Rel-rod dark field images did not reveal any faulted loops in the unirradiated ZrC. Bubbles approximately ~1 nanometer in diameter were identified in the previous study. The small bubbles are due to damage caused by ion milling with argon ions. No precipitates were

found in the unirradiated ZrC. A few scattered voids and line dislocations were found at low magnification, likely due to the fabrication process.

While the bright field image at the **g**=200 diffraction condition reveals defect feature similar to the unirradiated condition in Figure 5, the relrod weak beam dark field image shows the small faulted loops with a high density at the edge-on view. This is a significant change from the unirradiated sample. The measured average size and density for the faulted loops is 7.2 nm and $4.2x10^{16}$ cm^{-3}, respectively. The size distribution of the faulted loops is plotted in Figure 6, indicating a loop size range of 3 – 16 nm. A careful examination of the bright field image for the irradiated ZrC reveals extra features of the small straight lines oriented in certain directions due to the presence of the faulted loops. No radiation induced voids or amorphization are found in ZrC irradiated with protons at 800 °C to 3.0 dpa

The HOLZ patterns at zone [114] for the unirradiated ZrC and the simulated matching pattern are shown in Figure 7. The lattice constant for the unirradiated ZrC is estimated to be 0.469 nm with 0.2% uncertainty, slightly smaller than the data of 0.473 nm in literature [11]. The details of the HOLZ line patterns are clearly displayed in the unirradiated ZrC. There is no significant degradation on the visibility of HOLZ pattern for ZrC irradiated with proton at 800°C to 3 dpa. To evaluate the possible lattice constant change due to irradiation, a comparison of the HOLZ line pattern between the unirradiated and the irradiated ZrC is shown in Figure 8. Both patterns look identical, indicating the lattice constant change within the uncertainty limit of 0.2%.

ZrN

The microstructure of the unirradiated and irradiated ZrN is shown in Figure 9. Similar to the unirradiated ZrC, the microstructure for the unirradiated ZrN reveals clear evidence of ion milling damage. There are a few areas with precipitates, scattered voids and dislocation lines. EDS revealed the circular shaped precipitates (typically < 200 nm) are rich in Zr and O and are believed to be ZrO_2. A few large polygon shaped precipitates (typically > 1 μm) at grain boundaries are also observed. These precipitates are rich in Al and O with an atomic ratio near 2:3 and are likely Al_2O_3. The diffraction pattern and Kikuchi line pattern for the unirradiated ZrN is clear despite the defects produced by ion milling damage.

For the irradiated ZrN, the microstructure reveals no significant changes in bright field images of the defects shown in Figure 9. No dislocation loops (faulted or perfect) are identified. The relrod weak beam dark field image did not show any faulted loops. The fine white spots in the relrod image are likely due to the black dot defects created both from irradiation and ion milling. Radiation induced voids, precipitates and amorphization are not found in the ZrN at 3.0 dpa. No extra spots are formed in the selected area diffractions.

HOLZ line pattern match has been used to measure the lattice constant for the unirradiated ZrN, shown in Figure 10. A lattice constant of 0.458 nm has been determined from the best match, consistent with the literature data of 0.4575 nm [10]. A comparison of HOLZ patterns between the unirradiated and the irradiated ZrN is shown in Figure 11. Similar to ZrC, there is no

discernable change between the unirradiated and the irradiated patterns. The lattice constant change due to irradiation is believed to be within the uncertainty limit of 0.2%.

SiC

For the hexagonal SiC there are many possible configurations due to the variation in its stacking sequence along the [0001] crystal direction. The SiC used in this work is a 6H-SiC, as depicted in Figure 1. The stacking sequence repeats after every 6 layers of Si along [0001]. For the unirradiated SiC, the microstructure is summarized in Figure 12. Most of the areas on the sample show uniform matrix with little evidence of ion milling damage from sample preparation in contrast to the unirradiated ZrC, ZrN, TiC and TiN. The microstructure is decorated with scattered dislocations and significant amount of stacking faults (See Figure 12, pictures on the top). Due to the large lattice constant (c=1.5117 nm), the projection of basal planes at the edge-on condition is clearly visible by imaging at zone [1,-2,1,0] without using the objective aperture (see Figure 12 pictures on the bottom). A close look at stacking faults reveals the spacing variation between the fringes due to stacking faults on basal plane [1].

For the SiC irradiated with protons at 800ºC to 1.5 dpa, irradiation-induced defects in comparison with that of the unirradiated SiC are shown in Figure 13. The bright field image with **g** = 006 shows the small black dot type of defects at high density in the irradiated sample. The high resolution view of the basal plan projection at magnification of 100K and 400K also reveals a significant increase in the number of defects in the irradiated SiC. Similar to the unirradiated case, stacking faults are still present as a main microstructure feature in the 1.5 dpa SiC. There is no noticeable degradation in the visibility of Kikuchi patterns in convergent bean diffraction for the irradiated SiC.

To evaluate if there is any lattice constant change due to irradiation, a comparison of the high resolution images for basal plane projection is shown in Figure 14. The match on the two sets of fringes between the unirradiated and the irradiated SiC indicates no change on the basal plane spacing. There is therefore no change in the lattice constant, c. The experimental HOLZ line patterns at zone [0001] for the unirradiated and the irradiated 6H-SiC are presented in Figure 15. The difference in the polygon fringes is due to the difference in the thickness where the HOLZ line pattern was recorded. There is no discernable difference in the HOLZ line patterns between the two conditions, indicating no lattice constant change.

Discussion

The discussion on the results of the proton irradiation (2.6 MeV, 800°C) will be contrasted with the results from the previous work using Kr irradiation (1 MeV, 800°C) on the same batch of ceramics. Note that there is a large difference (~ 10^3) in displacement damage rate between Kr ion and proton irradiation. It is worth mentioning that proton irradiation provides a displacement damage rate similar to the GFR core (~ 10^{-6} dpa/sec) with reasonable irradiated volume (depth ~ 30 μm) but is limited by its practically achievable dose (~ 10 dpa) while Kr ion irradiation has an advantage to achieve very high dose (~ 10^2 dpa) but is limited by the very small irradiated

volume (depth < 1 μm). Proton irradiation creates an irradiated microstructure representing bulk microstructural change. TEM sample preparation after proton irradiation prevents any surface effects on the microstructure from irradiation. This is a great advantage over the Kr irradiation where the thin area of a TEM sample is irradiated in-situ in an intermediate voltage electron microscope equipped with an accelerator.

ZrC

The faulted loops on the (111) planes are typical defect features in irradiated fcc metals. These loops are effective barriers to mobile dislocations and contribute significantly to radiation hardening in the materials. The small sizes and high density of these loops in ZrC irradiated at 800ºC is likely due to the relative low irradiation temperature compared to its melting point ($T_{irr}/T_m = 0.28$) [12]. The size distribution of these small loops is typical in irradiated materials. The previous Kr ion irradiation at 800ºC to both 10 and 70 dpa did not reveal faulted loops. It was thought the crystal structure in ZrC (two sets of fcc structures overlapping) was responsible for the lack of faulted loops. Knowing the difference of 3 orders of magnitude in displacement damage rate, proton irradiation seems more effective in producing faulted loops for the given irradiation temperature. This is possibly due to the kinetics for interaction and migration of point defects and defect clusters in favor of faulted loop formation. Unlike the Kr ion irradiated ZrC, a ring pattern in the selected area diffraction is not observed in the proton irradiated sample. This suggests the microstructure evolution in proton irradiation is relatively simple than in Kr ion irradiation. It is realized that the previous microstructure analysis is complicated by the surface problems such as oxidation created during Kr ion irradiation.

Although small bubbles existed in the unirradiated sample from ion milling with Ar ions, the lack of void development in the proton irradiated ZrC may be attributed to both the low irradiation temperature and crystal structure for ZrC. In fcc metals, void formation typically occur in an intermediate temperature range ($T_{irr}/T_m = 1/3 \sim 1/2$). The results of the proton irradiation is consistent with Kr ion irradiation where no voids were found even at doses up to 70 dpa. Unlike the fcc metals, the crystal structure of ZrC can be envisioned as a fcc lattice of Zr with C filling in the octahedral interstitial sites. Irradiation produces point defects and defect clusters in the material. The evolution of these defects and clusters under radiation-enhanced diffusion, plus the interactions of these defects with various sinks, determines the irradiated microstructure. According to the work by Li [13] on the inter atomic potential of ZrC, the properties of ZrC are dominated by the strong covalent bonds and the weak ionic bonds (Zr-C) and the original metallic bonds (Zr-Zr) can be neglected. It is possible that this unique structure and strong chemical bonding may significantly slow down the diffusion and increase the formation energy for both voids and faulted loops. Radiation induced amorphization is not identified in either the proton, or Kr ion irradiations at 800ºC, indicating the crystal structure is stable against amorphization at the given irradiation temperature.

The visibility of the Kikuchi pattern and HOLZ line pattern in convergent beam electron diffraction may be used to qualitatively evaluate the crystal structure integrity. It seems the latter is more sensitive to the distortion on the crystal atomic planes in the lattice. In ZrC irradiated with protons to 3.0 dpa, there is no noticeable degradation on the visibility of both Kikuchi pattern and HOLZ line pattern. This is in contrast to Kr ion irradiation where the visibility of

the Kikuchi pattern degrades noticeably at 10 dpa and severely at 70 dpa while the visibility of HOLZ line pattern already drops to zero at 10 dpa. These comparisons suggest that the crystal atomic plane suffer less distortion from irradiation with protons to 3.0 dpa than with Kr ions to 10 dpa. This allows the use of HOLZ patterns to measure the lattice constant and its changes in the proton irradiation case with much less uncertainty (0.2%) compared to the use of the select area diffraction pattern which may carry an uncertainty greater than 1% likely due to the difficulty in sample height control in the TEM even with good alignment and calibration [7].

The measured lattice constant (a=0.469 nm) using the HOLZ line pattern is slightly smaller than the literature data (a=0.473), possibly due to the presence of 2% Hf in the material. Comparison of the HOLZ line patterns between the unirradiated and the irradiated condition shows no noticeable difference, indicating a lattice constant change less than 0.2%. This result is inconsistent with neutron irradiated ZrC at 130-355ºC to 7.5 dpa where a 2.5% volume increase is observed and believed mostly caused by the defect clusters [2]. Unfortunately there is no microstructural analysis for their work. It is anticipated that neutron irradiation to 7.5 dpa will produce more damage to microstructure than proton irradiation to 3.0 dpa at comparable temperature. The large difference in the irradiation temperature between proton and neutron data makes the comparison difficult and it is hard to draw any meaningful conclusion. This is a typical case for radiation study on GFR ceramics since the reference data on radiation performance for these candidate ceramics under irradiation conditions relevant to GFR cores does not exist.

ZrN

The major difference between the proton irradiated ZrC and ZrN is the lack of faulted loops in ZrN. The Kr ion irradiation also reveals large difference in microstructural response to irradiation between ZrC and ZrN in a different aspect. It suggests that carbides and nitrides act significantly differently in the microstructure evolution under irradiation. The exact cause for the lack of faulted loops in ZrN is not clear. One obvious explanation is that nucleation of faulted loops is more difficult in ZrN than in ZrC. Similar to ZrC, no radiation induced amorphization or precipitation is observed in the proton irradiated ZrN.

While Moire fringes and ordered fcc structure developed as major features in Kr ion irradiated ZrN, none of these features are found in the proton irradiated ZrN. Like ZrC, the visibility for Kikuchi pattern and HOLZ line pattern under convergent beam electron diffraction for proton irradiated ZrN show no discernable degradation. For Kr ion irradiated ZrN the visibility for HOLZ line pattern drops to zero and for Kikuchi patterns degrades at 10 dpa. The comparison indicates proton irradiation to 3.0 dpa causes less distortion on the lattice than Kr irradiation to 10 dpa for ZrN, consistent with proton irradiated ZrC. It is believed that the surface problem developed in Kr ion irradiated ZrN may be partially responsible for its complex microstructural evolution under irradiation. Note that the microstructure analysis for proton irradiated sample completely eliminates any surface problem by examining the irradiated volume approximately 15 μm away from the irradiated side.

The lattice constant measured (a = 0.458 nm) using the HOLZ line pattern at zone [114] is in excellent agreement with the literature data (a = 0.4575 nm). The comparison of HOLZ patterns between the unirradiated and the irradiated ZrN shows no noticeable changes in line pattern. This indicates the change in lattice constant due to proton irradiation is less than 0.2%. Similar to ZrC, no compatible case for neutron irradiation can be found in the open literature for a meaningful comparison.

SiC

In the following discussion, SiC refers to 6H-SiC unless otherwise specified. The difference in the unirradiated microstructure between SiC and the other ceramics is obvious by comparison of Figures 5, 9 and 12. The microstructure characterization for the unirradiated SiC suggests that SiC has the least radiation damage from ion milling among the 5 ceramics. SiC has the largest unit volume (0.1242 nm^3), lowest molecular weight (40.1) and the smallest atomic size when comparing the Si case to Ti and Zr. These differences may be partially responsible for its good resistance to the ion milling damage during sample preparation. The scattered dislocations in the unirradiated SiC may be due to materials fabrication. The high density of stacking faults in 6H-SiC is a common feature in microstructure for this material. Although some details of the projection of atomic layers along [0001] direction are revealed by the high resolution image at zone [1,-2,1,0], as shown in Figure 12, a high quality high resolution image with much more details on atomic arrangement can only be obtained by using a dedicated high-resolution TEM microscope.

The comparison of the microstructure between the unirradiated and the irradiated SiC (1.5 dpa) reveals the presence of black dot type defects at high density, Figure 13. The chemical and crystal structure analysis for these small defects was not successful due to their small size and limitations of the microscope. Some of these small defect features may be loop embryos. But no well defined loops can be identified. In the Kr ion irradiation work, well defined loops only show in the SiC irradiated to 70 dpa. According to the work by Persson [5], these loops are most likely interstitial loops residing on (0001) planes. Since loops only developed at very high dose in Kr irradiated SiC, the dose for proton irradiation to 1.5 dpa may be too low to see the loops. Considering the well defined defect features in proton irradiation at 1.5 dpa in contrast to the relatively clean microstructure after Kr irradiation at 10 dpa, proton irradiation seems more effective in producing microstructure damage than Kr ions in SiC.

The lattice constant change from proton irradiation is examined using both high resolution images of basal plane projection at zone [1,-2,1,0] and the HOLZ patterns at zone [0001]. The comparison of the fringe spacing from high resolution images of basal plane projection indicates no change from proton irradiation in the lattice constant, c, as shown in Figure 14. The HOLZ line patterns look identical between the unirradiated and the proton-irradiated SiC, suggesting the lattice constant change less than 0.2%. This is consistent with the result from Kr ion irradiation where lattice constant change was not seen even at 70 dpa using selected area diffraction pattern. Proton irradiation to 1.5 dpa for SiC shows no effect on the visibility of both Kikuchi pattern and HOLZ pattern.

Conclusion

Proton irradiation at 800ºC to 3.0 dpa in ZrC produced small faulted loops at high density. No loops are found in the ZrN irradiated under the same condition. HOLZ line patterns are clearly visible in ZrC and ZrN irradiated with protons to 3.0 dpa, but not in the same ceramics irradiated with Kr ions to 10 dpa. This may be attributed to the lower dose achieved in the proton irradiation for these ceramics. Proton irradiation produced uniformly distributed black dot type defects in SiC at 1.5 dpa, in contrast to Kr ion irradiation where no visible radiation induced defect features were observed at 10 dpa. The well defined defect features in proton irradiated ZrC and SiC suggests that protons are more effective at producing radiation damage in microstructure than Kr ions at 800ºC. Unlike the complex microstructural response obtained with Kr irradiation in the previous work, the irradiated microstructure in proton irradiation is relatively simple, possibly due to the lower dose and the benefit of eliminating the adverse surface problem.

The use of HOLZ line patterns in proton-irradiated ceramics allows accurate determination of the lattice constant and its changes in the three ceramics investigated. The comparison with HOLZ line patterns between the unirradiated and the irradiated ceramics indicates no change in lattice constant within an uncertainty limit of 0.2%. While 6H-SiC was identified as the best ceramics based on the microstructural stability under Kr irradiation among the 5 ceramics in the previous work, the same conclusion can not be made in this proton irradiation study, possibly due to the relatively low dose. In this work, ZrN shows less microstructural change to proton irradiation as compared to ZrC and SiC.

Acknowledgement:

The authors like to express their gratitude to Clayton Dickerson, Brandon Miller Hannah Yount and Kim Kriewaldt at the University of Wisconsin Ion Beam Laboratory for the proton irradiation. This work was funded by the U.S. Department of Energy through the Generation IV program on GFR Materials at Idaho National Laboratory.

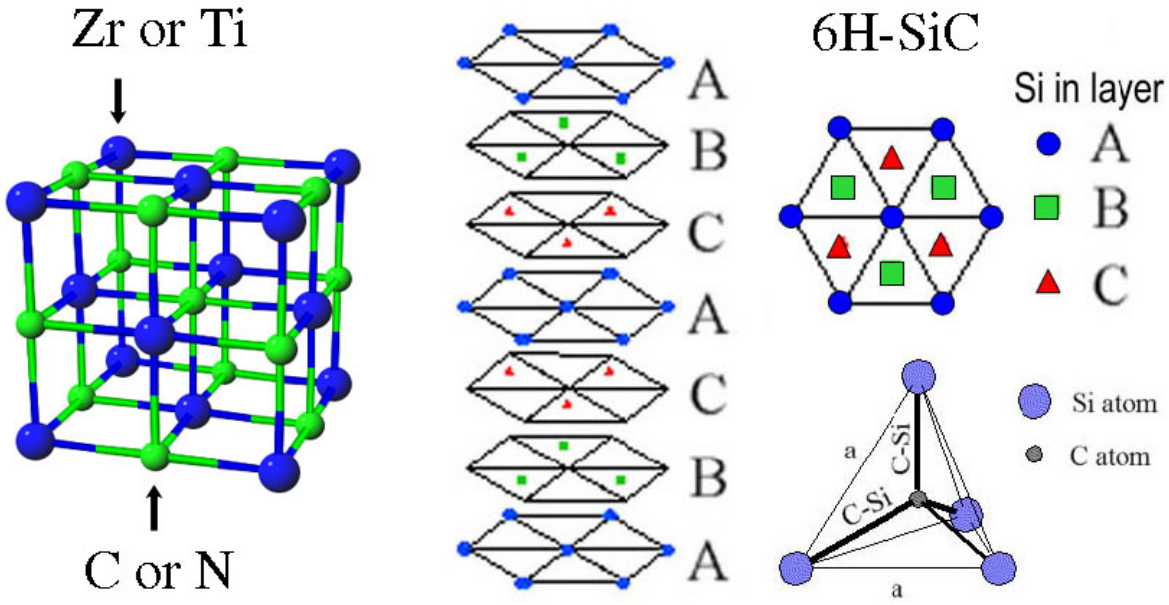

Figure 1. Atomic arrangement of the NaCl type FCC crystals for ZrC, ZrN, TiC and TiN (left) and the hexagonal crystal for 6H-SiC (right). Note that the stacking sequence in 6H-SiC repeats after every 6 layers.

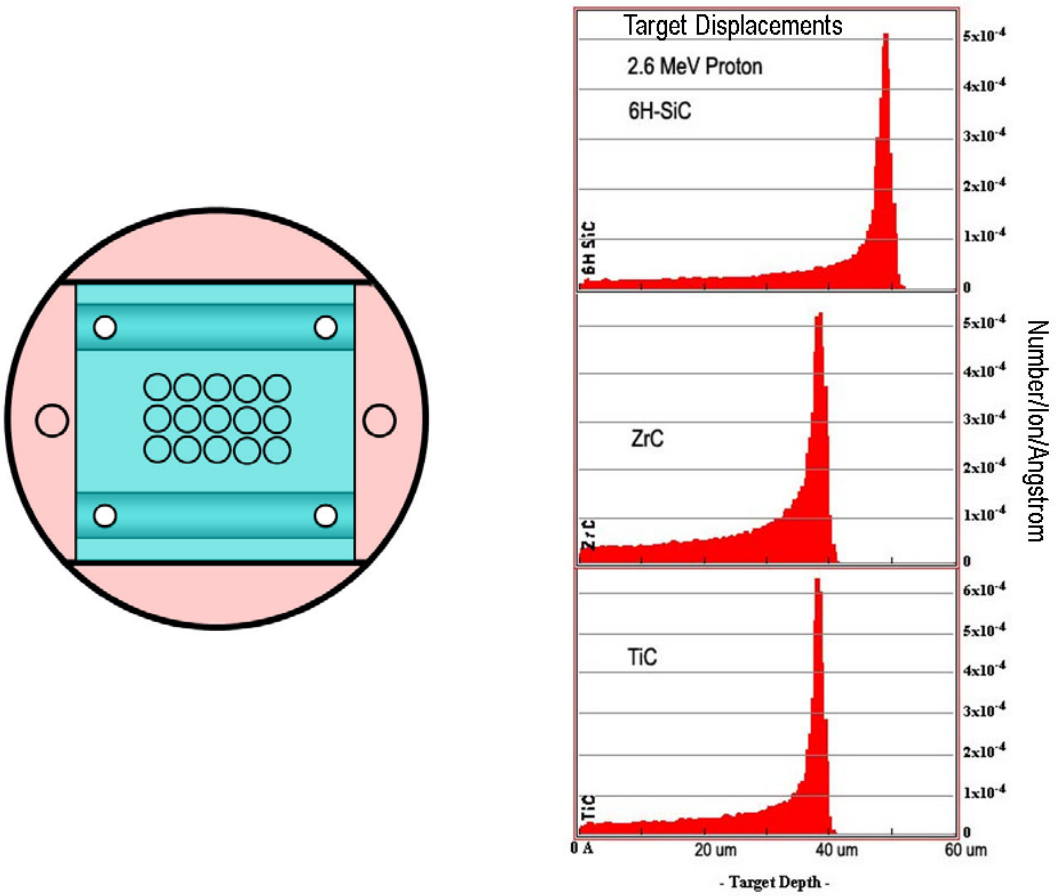

Figure 2. Disc sample loading on the irradiation stage (left) and the calculated displacement damage profile (right).

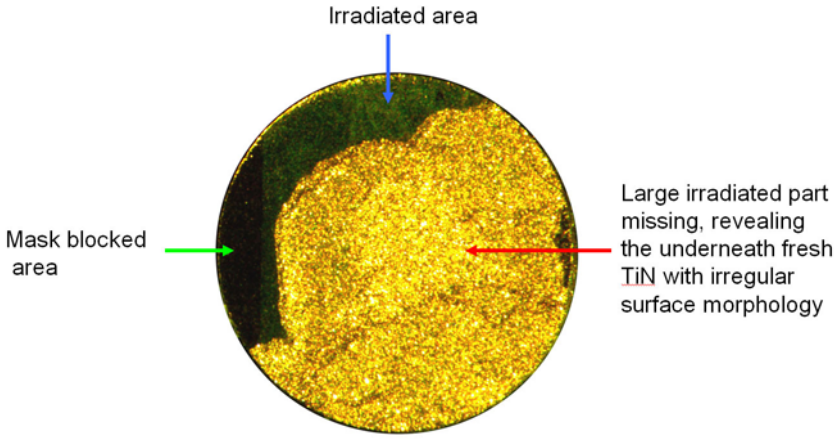

Figure 3. Sample surface condition for the irradiated side of TiN discs, showing most of the irradiated area is missing due to cracking.

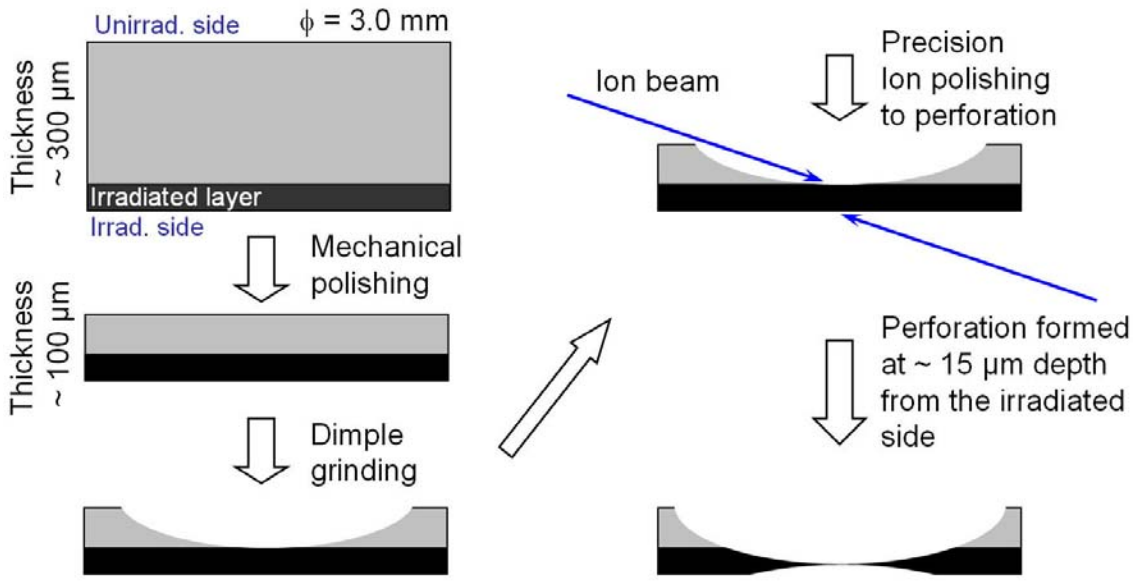

Figure 4. Illustration of TEM sample preparation for proton-irradiated ceramic discs.

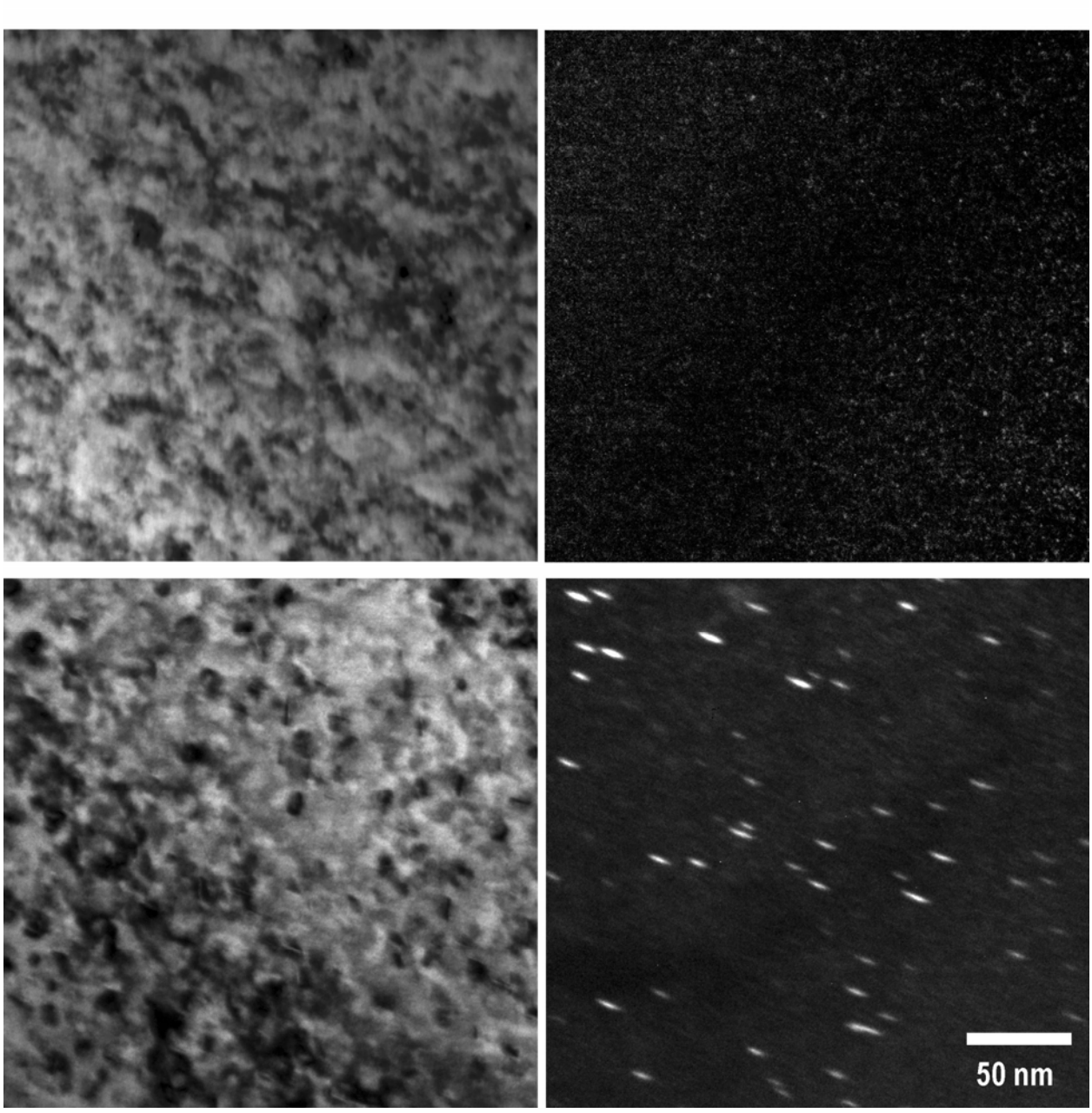

Figure 5. Microstructure of the unirradiated ZrC (top) and the irradiated ZrC (bottom) imaged with **g**=200 near zone [011] (left) showing black dot damage from ion milling and the rel-rod weak beam dark field image (right) showing faulted loops only in the proton-irradiated ZrC (800ºC to 3.0 dpa).

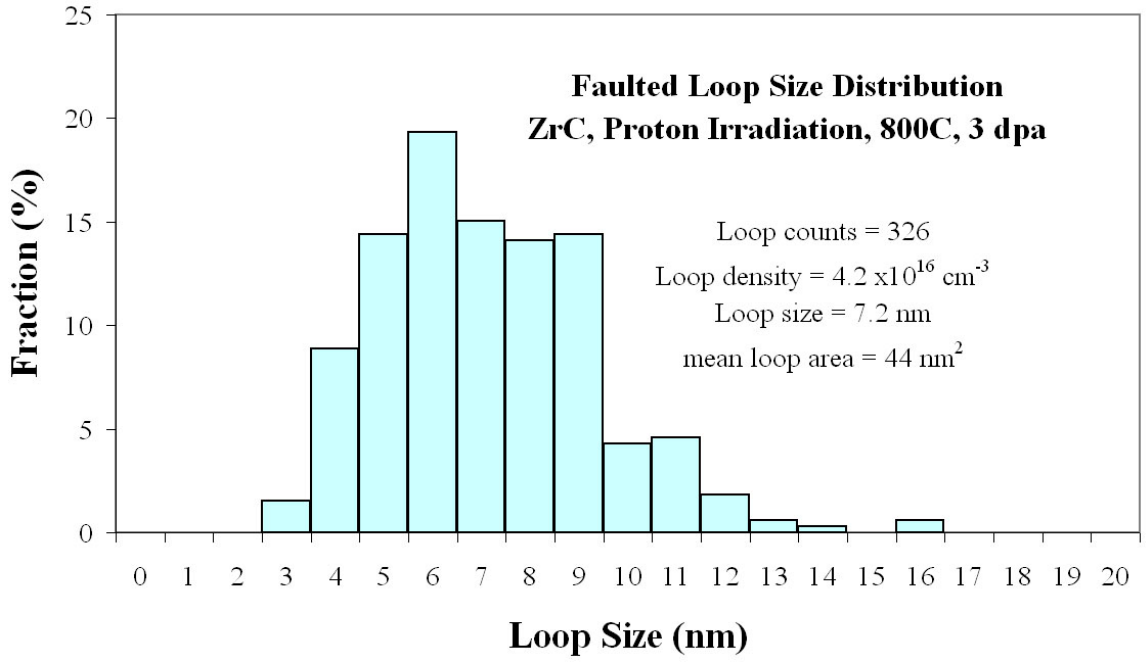

Figure 6. Size distribution of the faulted loops in ZrC irradiated with protons at 800 ºC to 3.0 dpa.

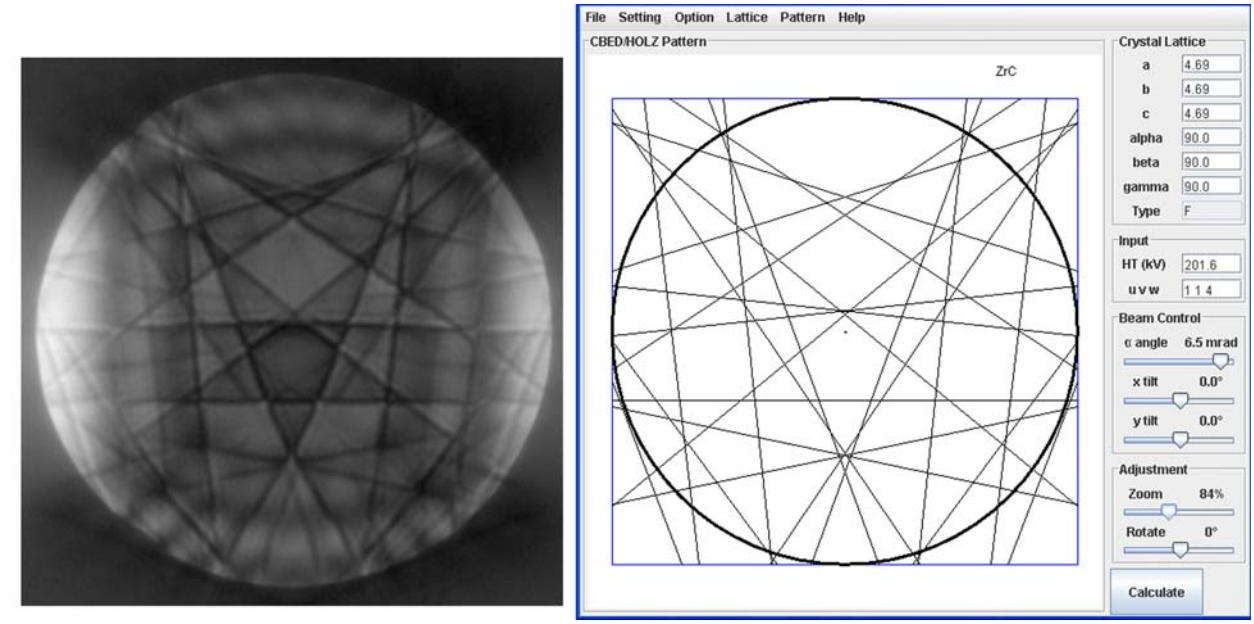

Figure 7. Comparison of HOLZ experimental pattern (left) and the simulated pattern (right) for ZrC at zone [114] showing a good match with a lattice constant of 0.469 nm. The accelerating voltage is calibrated using a single crystal Si (a_0 = 0.5437 nm).

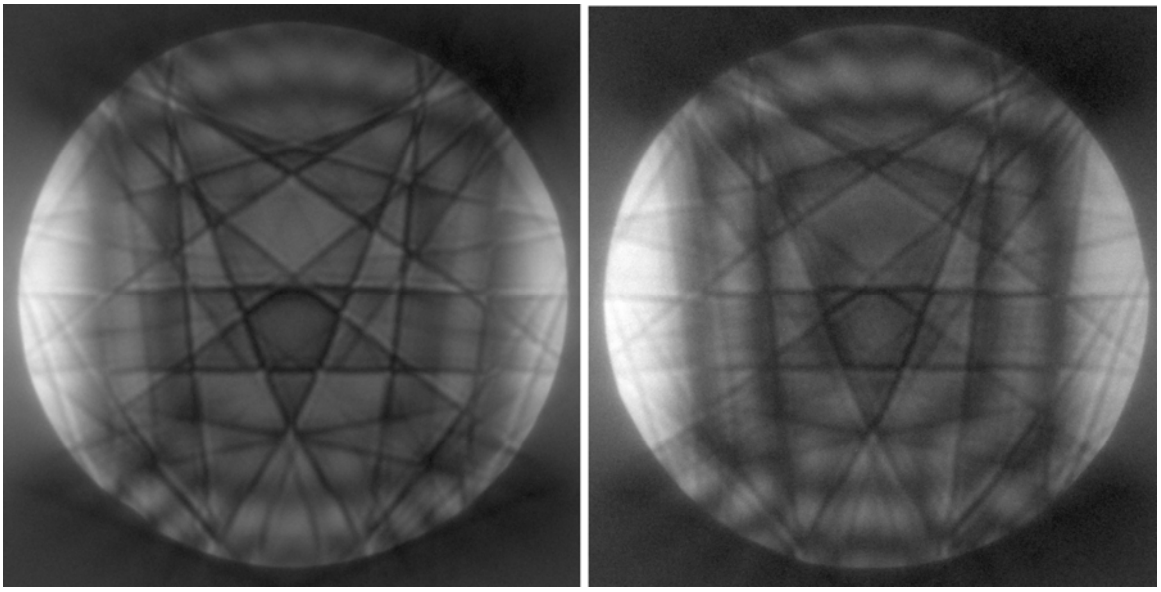

Figure 8. Comparison of HOLZ patterns at zone [114] for the unirradiated ZrC (left) and irradiated ZrC (right) with protons at 800°C to 3.0 dpa, showing no noticeable change in lattice constant.

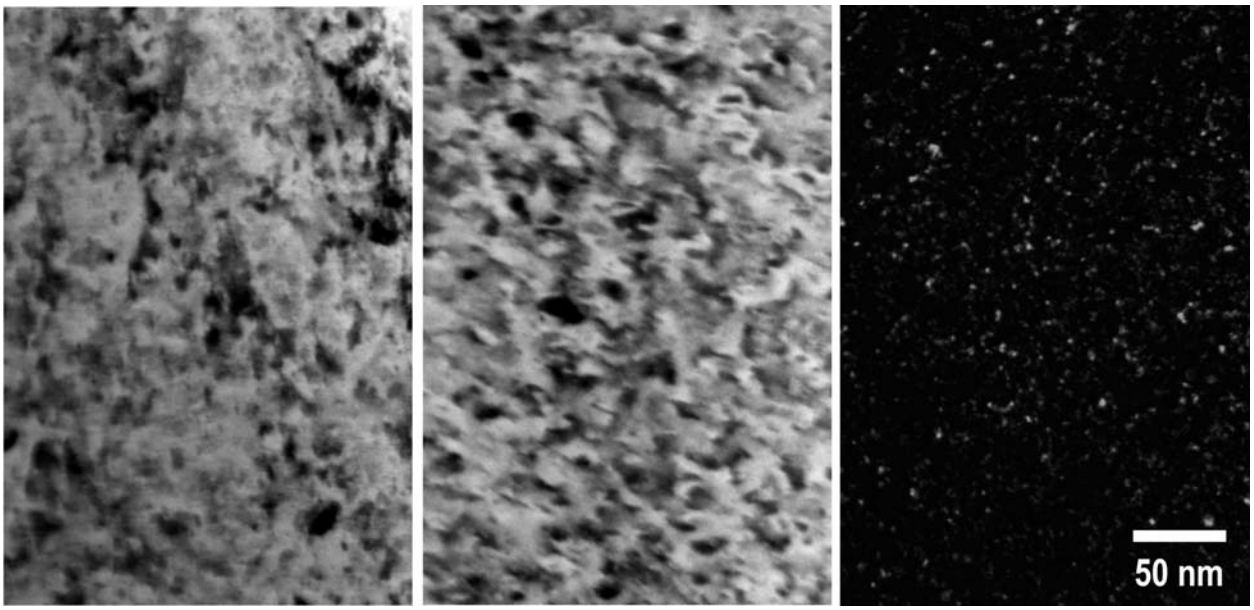

Figure 9. Microstructure of unirradiated ZrN (left) and the irradiated ZrN (middle) imaged with **g**=200 near zone [011]. Faulted loops are not found in the relrod weak beam dark field image in the ZrN irradiated with protons at 800°C to 3.0 dpa (right).

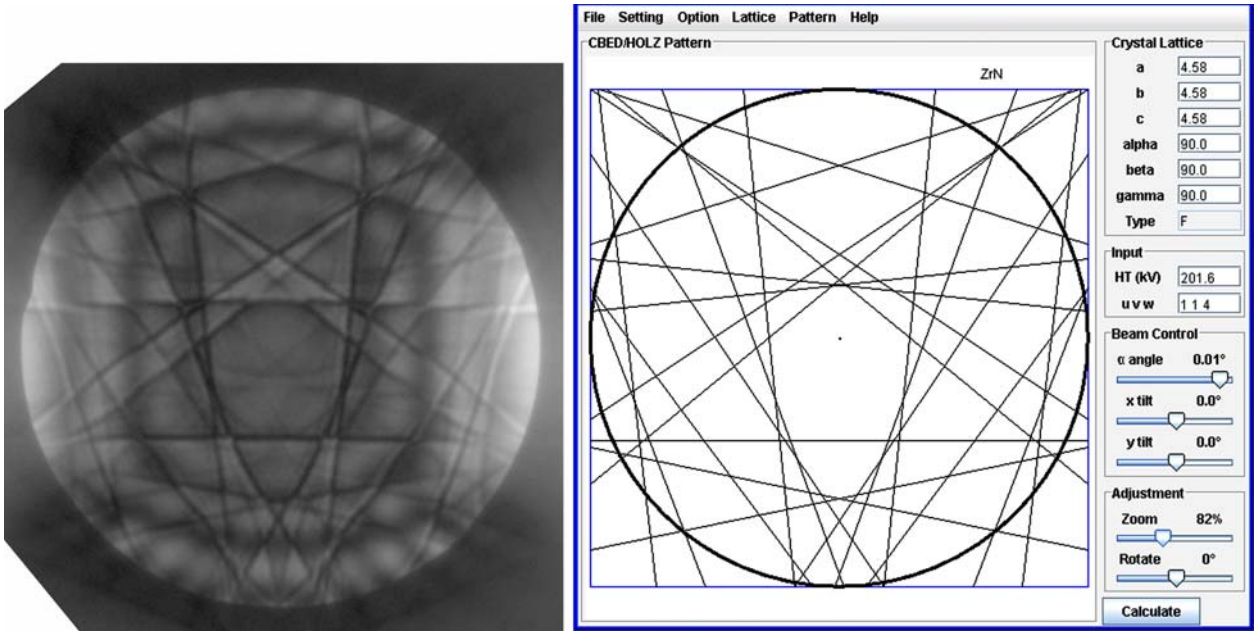

Figure 10. Comparison of HOLZ experimental pattern (left) and the simulated pattern (right) for ZrN at zone [114] showing a good match with a lattice constant of 0.458 nm.

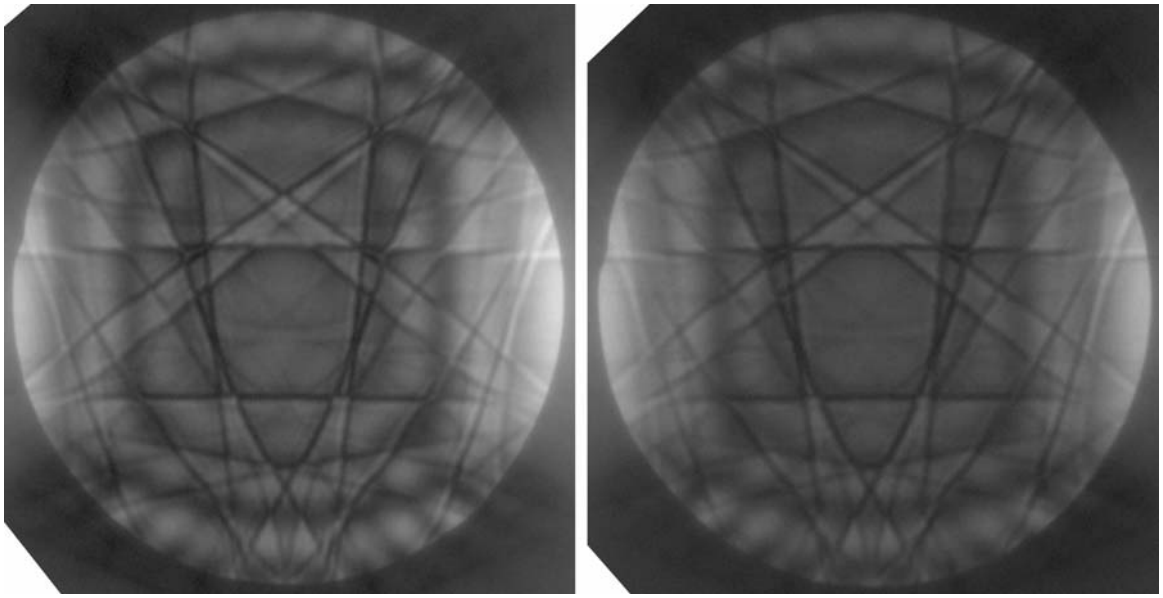

Figure 11. Comparison of HOLZ patterns at zone [114] for the unirradiated ZrN (left) and irradiated ZrC (right) (800°C to 3 dpa), showing no noticeable change in lattice constant.

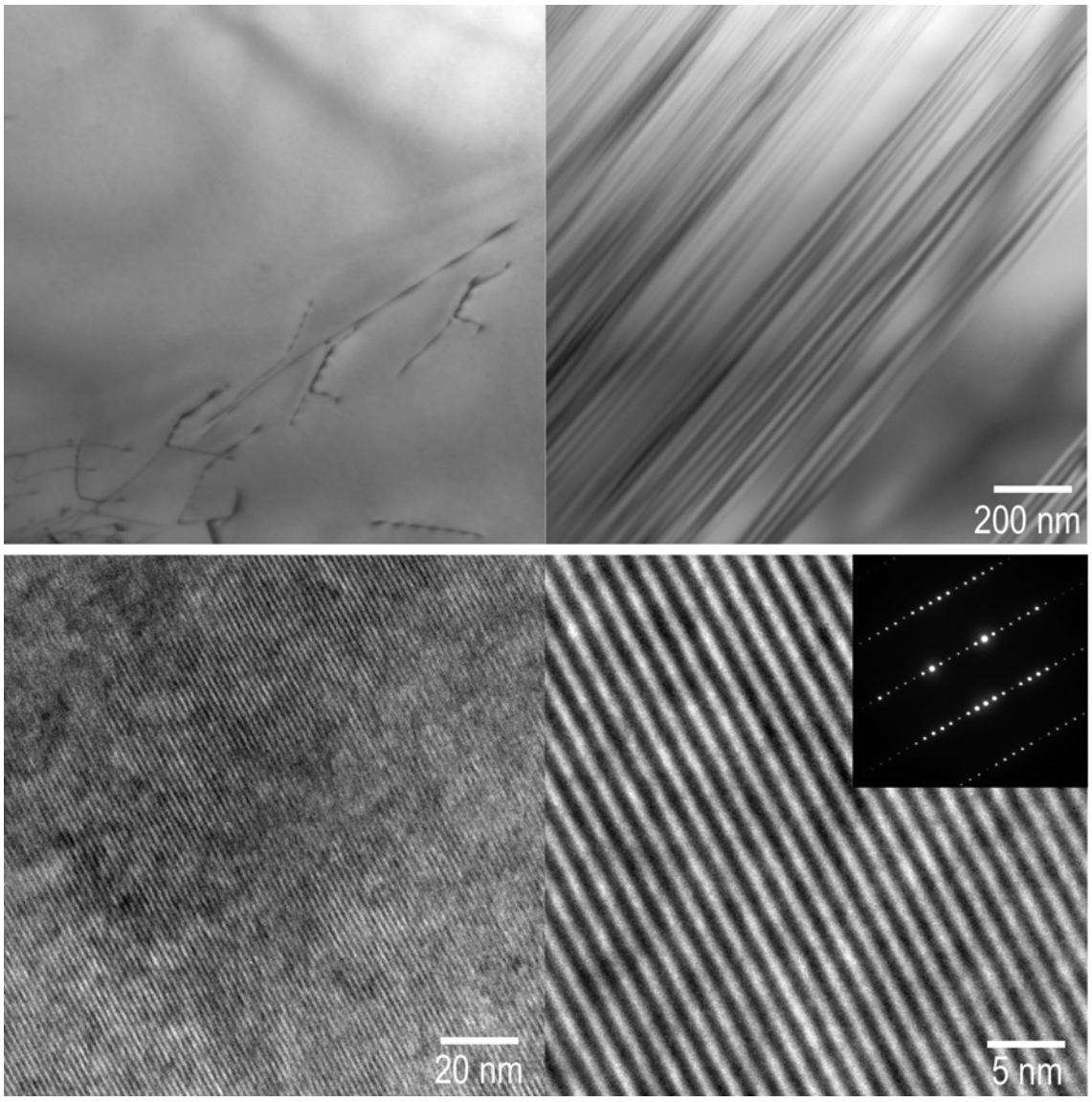

Figure 12. Microstructure of the unirradiated 6H-SiC. It shows scattered dislocations (top-left) and a group of stacking faults (top-right). The high resolution images (bottom) reveal the projection of basal planes at edge-on condition. The insert shows the diffraction at zone [hkil]=[1,-2,1,0] which is used to form the high resolution
.

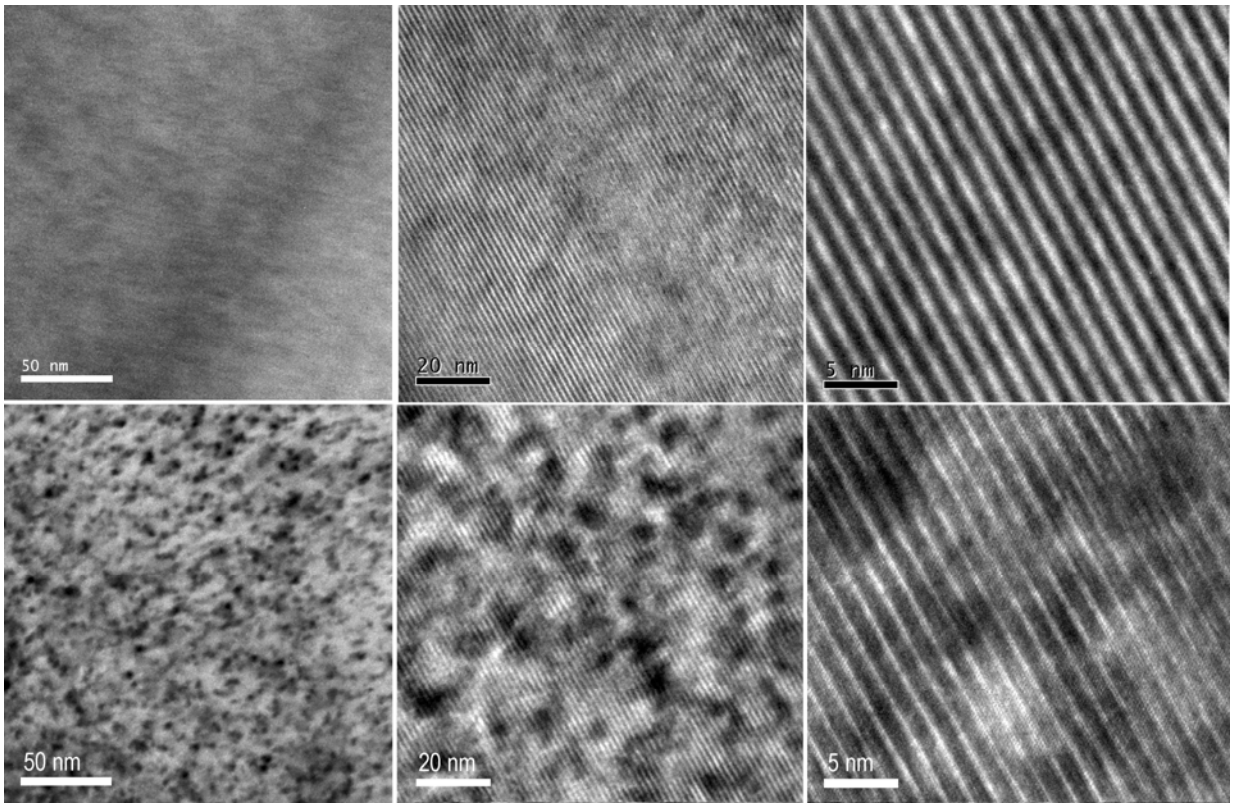

Figure 13. Comparison of microstructure for the unirradiated (top) and proton-irradiated (bottom, 1.5 dpa) 6H-SiC in bright field images with g = 006 (left) and high resolution images at zone [1,-2,1,0] showing defects and projection of basal planes (middle and right).

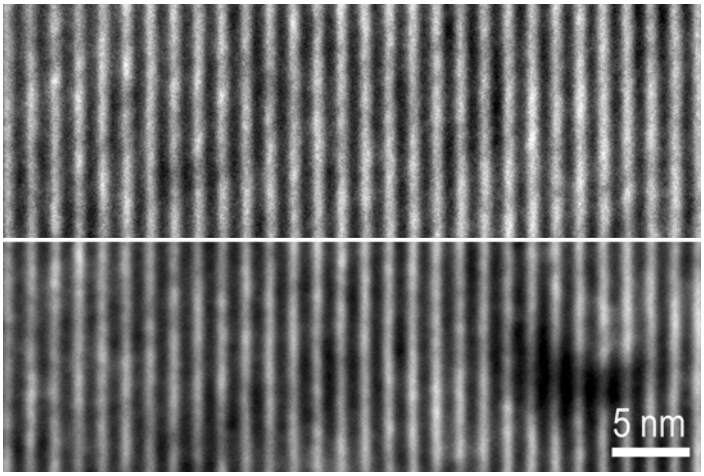

Figure 14. Comparison of high resolution images of basal plane projection between the unirradiated (top) and irradiated 6H-SiC (bottom) at zone [1,-2,1,0], showing no change in basal plane spacing from proton irradiation at 800ºC to 1.5 dpa.

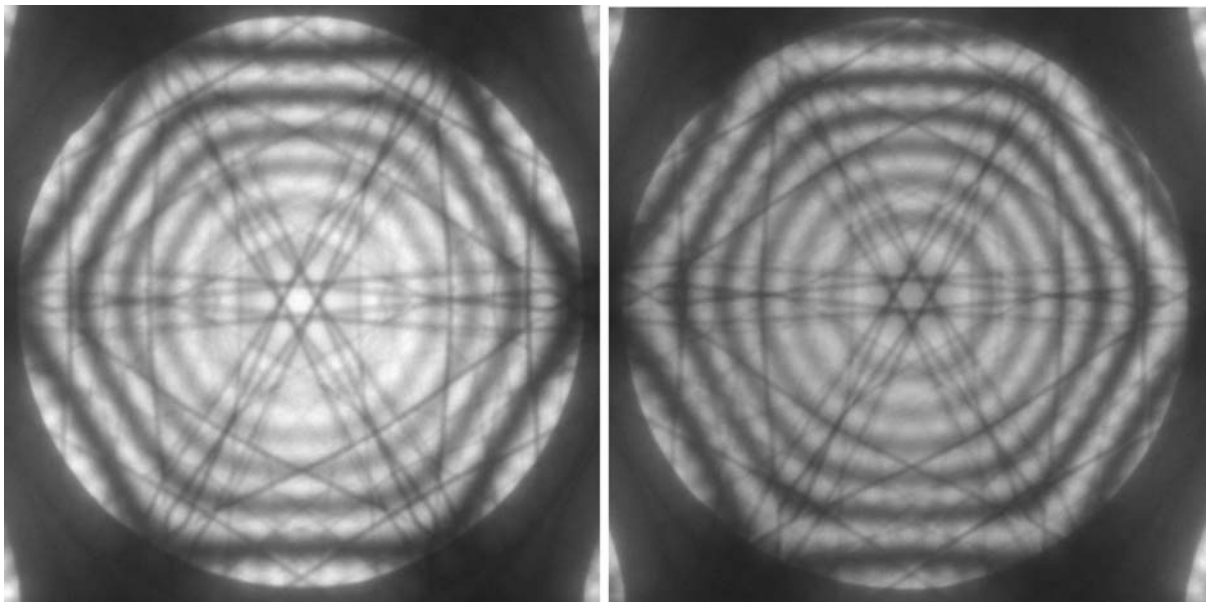

Figure 15. Comparison of HOLZ line patterns at zone [0001] between the unirradiated (left) and the irradiated 6H-SiC (right, 1.5 dpa at 800°C), showing no change in lattice constant.

Reference:

[1] J. Gan, R. Fielding, M. K. Meyer and B. C. Birtcher, "Ion Irradiation Study on Microstructure Stability of GFR Ceramics: ZrC, ZrN, TiC, TiN and SiC Irradiated with 1 MeV Kr ions to 10 and 70 dpa at 800ºC", FY 2005 Summary Report for DOE Gen-IV program on GFR Materials, 2005.
[2] D. A. Dyslin, R. E. Moore and H. E. Robertson, ORNL-4480 (1969) p245
[3] W. J. Weber, L. M. Wang and N. Yu, Nucl. Instr. Methods in Phys. Research B., 116 (1996) 322
[4] P. O. A. Persson, L. Hultman, M.S. janson and A. Hallen, R. Yakimova,, Journal of Applied Physics, V. 93, #5, (2003) 9395
[5] P. O. A. Persson, L. Hultman, M.S. janson and A. Hallen, R. Yakimova, D. Panknin and W. Skorupa., Journal of Applied Physics, V. 92, #5, (2002) 2501
[6]J.F. Ziegler, J.P. Biersack and U. Littmark, The Stopping and Range of Ions in Solid, Pergamon Press, New York, 1996.
[7] D. B. Williams and C. B. Carter, "Transmission Electron Microscopy", Plenum Press, New York and London, 1996. p339
[8] J. C. H. Spence and J. M. Zuo, "Electron Microdiffraction", Plenum Press, New York and London, 1992
[9] X. Z. Li, "JECP/HOLZ – an interactive computer program for simulation of HOLZ patterns", Journal of Applied Crystallography, 38 (2005) 576
[10] W. Lengauer, S. Binder, K. Aigner, P. Ettmayer, A. Guillou, J. Debuigne & G. Groboth, J. Alloys Compds., 217 (1995) 137-1
[11] K. Aigner , W. Lengauer, D. Rafaja &, P. Ettmayer, J. Alloys Compds., 215 (1994) 121-1
[12] Binary Alloy Phase Diagrams, 2nd Ed., Editor: T. B. Massalaski, H. Okamoto, P. R. Subramanian and L. Kacprzak, ASM International
[13] J. Li, J. Appl. Phys., Vol. 93, No. 11 (2003) 9072